Intermetallics 59 (2015) 23–31

Contents lists available at ScienceDirect

Intermetallics

journal homepage: www.elsevier.com/locate/intermet

Review

Microstructure and chemical characterization of the intermetallic phases in Cu/(Sn,Ni) diffusion couples with various Ni additions

Anna Wierzbicka-Miernik [a, *], Krzysztof Miernik [b], Joanna Wojewoda-Budka [a], Lidia Litynska-Dobrzynska [a], Grzegorz Garzel [a]

[a] Institute of Metallurgy and Materials Science, Polish Academy of Sciences, 25 Reymonta Str., 30-059 Cracow, Poland
[b] Institute of Materials Engineering, Cracow University of Technology, 37 Jana Pawla II Av., 31-864 Cracow, Poland

ARTICLE INFO

Article history:
Received 5 September 2014
Received in revised form
3 November 2014
Accepted 1 December 2014
Available online 26 December 2014

Keywords:
A. Intermetallics
C. Joining
D. Microstructure
F. Electron microscopy, scanning
F. Electron microscopy, transmission

ABSTRACT

The paper presents new results concerning the influence of nickel addition (1 and 5 at.%) into tin on the development of the Cu/(Sn,Ni) interface area in diffusion couple experiment. The morphology and chemical composition of the intermetallic phases growing in the Cu/(Sn,Ni) diffusion couples were examined by means of the scanning (SEM) and transmission (TEM) electron microscopy after annealing at 215 °C in vacuum for different period time.

It was shown that even 1 at.% of nickel addition into tin resulted in formation of intermetallics of complex microstructure. The presence of $(Cu_{1-x}Ni_x)_6Sn_5$ in two morphological and compositional variants was noted. The discontinuous layer consisting up to 7.2 at.% of Ni closer to copper end-member coexisted with needle-like and faceted precipitates with even 22.3 at.% of Ni, which intensively detached from the interface. At the Cu/$(Cu_{1-x}Ni_x)_6Sn_5$ interface the formation of Cu_3Sn wavy layer compound was observed in all examined diffusion couples which became thicker with time. The porosity within the both formed intermetallic phases existed irrespective of the amount of added nickel.

1. Introduction

Soldering of modern materials is one of the main streams of the environment friendly technologies, which are nowadays intensively developed. The lead containing solders (Sn–Pb eutectic alloys), although widely used due to their good mechanical properties and low manufacturing cost, must be abandoned in the electronic industry [1]. The toxic effect of Pb on human health and the environment can no longer be ignored. Nowadays, it is particularly important to find environment friendly, non-toxic substitutes for the Pb high content solder materials in electronics [2].

At the present, the Sn based alloys with different ratio of Cu, Ag as additions, are the most common lead-free solders applied for copper soldering of electronic items. On the other hand, one of the surface plating used for printed circuit boards is electroless nickel–immersion gold (ENIG) and electroless nickel–electroless palladium–immersion gold (ENEPIG) [3]. There are also reports (for example [4]) describing the addition of nickel to lead-free solder such as SAC (SnAgCu) alloy only from the technological point of view. These experiments showed that very small addition of Ni as 0.01wt.% resulted in effective growth retardation of Cu_3Sn phase. Similar effect was caused by introducing of 0.05 wt.% Ni into Sn0.7Cu solder [5]. Such behavior was attributed to the accelerating interdiffusion through Cu_6Sn_5 and Cu_3Sn. On the other hand, the addition of 0.02–0.1 wt.% of Ni into Sn0.7Cu solder reacting with the Ni substrate, led to the morphology change of Cu_6Sn_5 (from cylindrical to faced) and its faster growth [6].

The other aspect of the Pb-free soldering is to find new methods that could fulfill more and more restrictive working conditions. The promising joining technology to be applied in the industry seems to be the diffusion soldering [7–11]. The goal of diffusion soldering is to obtain the joint fully filled by the intermetallic phase as in such a way the interconnection has a high thermal stability, reflecting the properties of the created intermetallic compound. In the existing literature data the diffusion soldering process took the significant time from minutes [12–14], hours [15] up to days [14,16] of interaction at high temperature. In particular the Cu/Sn/Cu diffusion soldered interconnection is important to recall to be later compared with presented results. Bader et al. [17] applied very thin (5.2 μm) tin layer sputter deposited on the copper substrate and annealed at

* Corresponding author. Tel.: +48 12 2952817; fax: +48 12 2952804.
E-mail address: a.wierzbicka@imim.pl (A. Wierzbicka-Miernik).

http://dx.doi.org/10.1016/j.intermet.2014.12.001
0966-9795/

240 °C for 20 min to obtain the joint totally filled by two intermetallics Cu_6Sn_5 and Cu_3Sn. With respect to this thickness such time of soldering is relatively long. In typical technological conditions such long soldering time is unrealistic, therefore the research is also focused on finding such additives to lead-free solders already applied, which will cause changes in the mechanism of phase transformations and in turn accelerate the formation and growth of the intermetallic phases.

Our previous study connected with the diffusion soldered interconnections demonstrated that small Ni addition (5 at.%) to the copper substrate changes not only the morphology but also the sequence of intermetallic compounds growing in the reaction zone. The microstructure and chemical composition analyses revealed only the formation of $(Cu,Ni)_6Sn_5$ phase, while no ε-Cu_3Sn was detected [10,11].

Similar behavior was also observed in the (Cu,Ni)/Sn diffusion couples. In the presence of 1 at.% Ni still $(Cu_{1-x}Ni_x)_6Sn_5$ and Cu_3Sn phases appeared but the reaction run faster compared to the classical Cu/Sn couples. Further addition of Ni (about 5 at.%) to copper led to the situation, that only growth of the $(Cu,Ni)_6Sn_5$ phase was observed [18,19].

The presented above examples are related for Ni addition to Cu substrate. Literature data provides the information concerning the Ni additions to SAC solder [20], SnAg [21] or reactions in Ni/SAC/Cu interconnections [22], where the different morphology of the $(Cu,Ni)_6Sn_5$ was reported. The present experiment is innovative in the light of the applied larger amounts of nickel additive (1 and 5 at.%) in comparison to the reported literature [20–22], where the Ni was up to 1 wt.% (usually 0.1 at.%). Moreover, solely the diffusion processes in the solid state are involved in the experiment. The goal of our study was characterization of microstructure and chemical composition of the phases which form and grow in the in the Cu/(Sn,Ni) diffusion couples (with 1 and 5 at.% of Ni).

2. Experimental

The Sn–Ni alloys for (Sn,Ni) pads were prepared by melting appropriate amounts of pure Sn (Alfa Aesar, 99.998%) and Ni (Alfa Aesar, 99.99%) in vacuum induction furnace (Leybold–Heraeus) under argon protective atmosphere (0.03 MPa) at the temperature 100 °C above liquidus, then cast into the steel mold to obtain ingots with the height of 90 mm and 15 mm of diameter. The same method was also applied for obtaining the pure Cu (Alfa Aesar, 99.99%) ingots with the similar shape. Next, the cast alloys were cut into slices with a thickness of 3 mm and then into quarters followed by grinding using a paper with a maximum gradation of 2000. Before the annealing, all the substrates were cleaned with acetone in an ultrasonic washer. Subsequently, the pieces of Cu and Sn–Ni alloys with 1 at.% and 5 at.% of Ni were pressed together and clenched in the specially prepared handle. The holder with the samples was placed in the quartz ampoule sealed under the vacuum and then placed in the muffle furnace heated up to the temperature of 215 °C (488 K) and annealed for different times: 48, 120, 168 and 225 h.

The cross-sections of the diffusion couples were prepared to characterize the morphology and chemistry of the intermetallic compounds growing in the reaction zone between Cu and (Sn,Ni) substrates.

The detailed studies of the formed intermetallic phases, their morphology and chemical composition were investigated using scanning electron microscopes: JEOL JSM 5510 LV equipped with an energy dispersive X-ray spectrometer (EDS), IXRF Model 500 as well as FEI Quanta 3D FEGSEM integrated with the EDAX Trident system.

The selected areas at the interfaces between the different phases formed in the examined diffusion couples, were cut out using a Quanta 3D Focused Ion Beam (FIB) to prepare the thin foils for the transmission electron microscopy (TEM) observations. The TEM investigations were performed using a TECNAI G2 FEG super TWIN (200 kV) microscope equipped with a high angle annular dark field detector and integrated with EDS system (Phoenix type) manufactured by EDAX.

Calculations of the binary equilibrium phase diagrams were accomplished based on the literature data [23] and with application of Pandat version 7.0.

3. Results

The SEM microstructure observations and the EDS analysis of the Cu/(Sn,Ni) diffusion couples with the 1 and 5 at.% of Ni addition, after annealing at 215 °C for 48, 120, 168 and 225 h in vacuum revealed the presence of three intermetallic compounds (IMCs) which were located in the following order: Cu pad/Cu_3Sn/$(Cu_{1-x}Ni_x)_6Sn_5$/$(Ni_{1-x}Cu_x)_3Sn_4$/(Sn,Ni) pad. The Ni_3Sn_4 phase was present in the (Sn,Ni) pad before the diffusion couples experiment in the form of single precipitates distributed in the shape of characteristic lines (Fig. 1a and b). Appearance of the phase results directly from the Sn–Ni binary phase diagram (Fig. 1c). Both of the selected compositions of the tin based substrates are located in the two-phase region: (Sn) + Ni_3Sn_4. However, in the case of 1 at.% of Ni addition the amount of this phase was negligible (Fig. 1a). It is worth noting that after 48 h of annealing the $(Ni_{1-x}Cu_x)_3Sn_4$ was located at the distance of about 400 μm away from Cu/(Sn,Ni) reaction zone (Fig. 2a). After longer annealing time this phase was placed beyond the area of the diffusion couple shown in Fig. 2b–d. The estimated distance of $(Ni_{1-x}Cu_x)_3Sn_4$ increased from 500 μm after 120 h to 800 μm after 225 h. Moreover, the chemical composition analysis revealed the diffusion of Cu far from the Cu/(Sn,Ni) interface and into the (Sn,Ni) pads because the grains of $(Ni_{1-x}Cu_x)_3Sn_4$ phase contained about 3 at.% of Cu far from the reaction zone and about 6 at.% closer to the center of diffusion couple (see Table 1). For the Sn + 5 at.% Ni composition of starting component more Ni_3Sn_4 phase was present and even after annealing the $(Ni_{1-x}Cu_x)_3Sn_4$ phase appeared in the form of small precipitates homogeneously distributed in the whole substrate (Fig. 3). The copper concentration in this phase changed from 2 at.% to 7 at.% when approaching to the reaction zone (Table 1).

Observation of the interface morphology of the diffusion couples revealed the formation of two new intermetallic phases. The use of EDS/SEM and TEM experiments allowed to identify them as $(Cu_{1-x}Ni_x)_6Sn_5$ and Cu_3Sn phases.

The $(Cu_{1-x}Ni_x)_6Sn_5$ phase was characterized by dual morphology. Close to the (Sn,Ni) pad grains of various shapes such as needle-type and faced one surrounded by the pure tin were formed while next to Cu_3Sn phase, the discontinuous layer of $(Cu_{1-x}Ni_x)_6Sn_5$ was present (Figs. 2 and 3).

The results of the EDS/SEM quantitative analysis of the phases within the investigated diffusion couples are collected in Table 1. The places of chemical point analyses were marked in Figs. 4 and 5 with numbers 1–10 and each of them represents the average values from several analyses.

This study showed the significant differences in the chemical composition within the $(Cu_{1-x}Ni_x)_6Sn_5$ phase dependent on its localization and morphology. In the case of the Cu/(Sn + 1 at.% Ni) diffusion couples the Ni concentration in the layer close to the Cu_3Sn phase reached 3–7 at.%, while in the large grains was much larger approaching 17–20 at.%. For the Cu/(Sn + 5 at.%Ni) diffusion couples these values were mostly the same. In the case of the grains

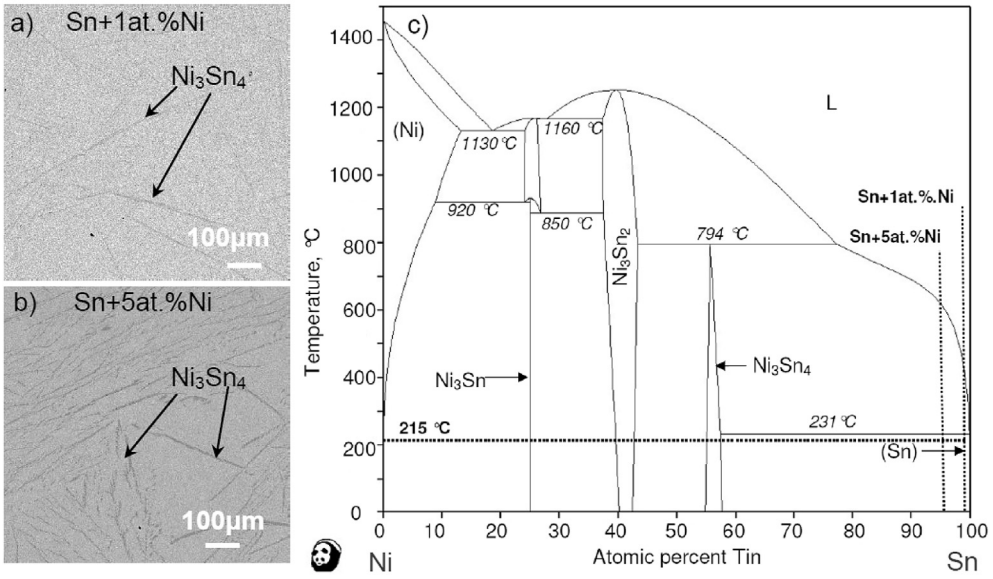

Fig. 1. (a and b) SEM micrographs of the (Sn,Ni) pads; (c) binary Ni–Sn phase diagram calculated based on data published in Ref. [23] with marked: annealing temperature – horizontal dashed line and compositions of the tin base pads – vertical dashed lines.

of the $(Cu_{1-x}Ni_x)_6Sn_5$ phase the nickel content was at the level of 22 at.% while in the layer it was found to be 4 at.%.

The SEM line scans analysis preformed for the samples annealed at 215 °C for 168 h (Fig. 6) clearly confirmed the variable nickel content in the $(Cu_{1-x}Ni_x)_6Sn_5$ phase. The obtained results showed also, that in the case of Cu_3Sn no Ni concentration was detected (Figs. 6 and 7) which corresponded to the point analysis of the chemical composition of the intermetallic phases (Table 1).

The transmission electron microscopy was applied in order to confirm identification of both intermetallics. Fig. 8a presents the localization of the thin foil (Fig. 8b) which was prepared using FIB method from Cu/(Sn + 5 at.%Ni) couple annealed at 215 °C for 48 h. Such methodology allowed to observe the Sn matrix (Fig. 8c) and all the phases existing across the Cu/(Sn,Ni) interface area namely: $(Cu_{1-x}Ni_x)_6Sn_5$ (Fig. 8d) and Cu_3Sn (Fig. 8e). Bright field image of the $(Cu_{1-x}Ni_x)_6Sn_5$ phase (Fig. 8d) revealed the presence of many

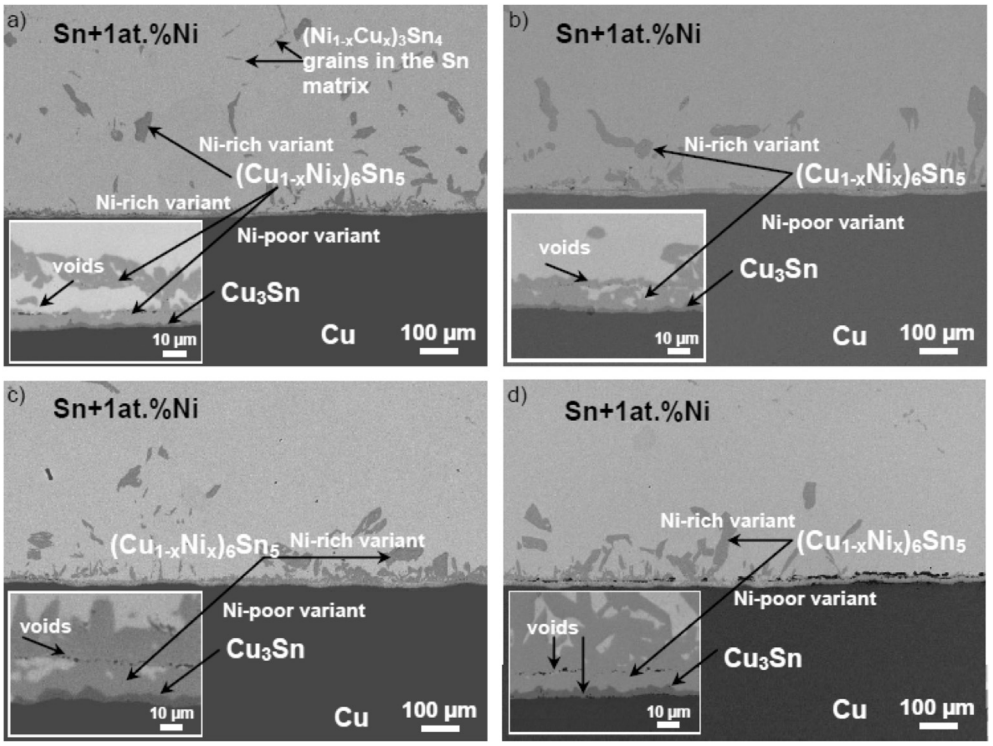

Fig. 2. SEM micrographs of the Cu/(Sn + 1 at.% Ni) diffusion couples annealed in vacuum at 215 °C for: (a) 48 h, (b) 120 h, (c) 168 h and (d) 225 h.

Table 1
The average values of the EDS/SEM quantitative analysis performed at points indicated in Figs. 4 and 5 in the Cu/(Sn + 1 at.% Ni) and Cu/(Sn + 5 at.% Ni) annealed at 215 °C for 168 h.

Point no.	Element content, at.%						Phase
	Cu/(Sn + 1 at.% Ni)			Cu/(Sn + 5 at.% Ni)			
	Cu	Ni	Sn	Cu	Ni	Sn	
1	3.1 ± 0.4	39.4 ± 0.8	57.5 ± 1.2	2.4 ± 0.2	40.3 ± 0.8	57.3 ± 1.1	$(Ni_{1-x}Cu_x)_3Sn_4$
2	6.1 ± 1.0	33.6 ± 1.3	60.3 ± 1.2	7.1 ± 1.4	33.1 ± 1.3	59.8 ± 1.2	$(Ni_{1-x}Cu_x)_3Sn_4$
3	33.4 ± 0.7	20.7 ± 0.8	45.9 ± 0.9	31.4 ± 0.6	22.3 ± 0.9	46.3 ± 0.9	$(Cu_{1-x}Ni_x)_6Sn_5$, Ni-rich variant
4	34.7 ± 0.7	19.4 ± 0.8	45.9 ± 0.9	31.7 ± 0.6	22.1 ± 0.9	46.2 ± 0.9	$(Cu_{1-x}Ni_x)_6Sn_5$, Ni-rich variant
5	36.8 ± 0.7	17.5 ± 0.8	45.7 ± 0.9	32.1 ± 0.6	21.6 ± 0.9	46.3 ± 0.9	$(Cu_{1-x}Ni_x)_6Sn_5$, Ni-rich variant
6	1.1 ± 0.2	0.3 ± 0.2	98.6 ± 2.0	1.2 ± 0.2	0.5 ± 0.3	98.3 ± 2.0	(Sn)
7	46.6 ± 0.9	7.2 ± 0.3	46.2 ± 0.9	49.3 ± 1.0	4.0 ± 0.5	46.7 ± 0.9	$(Cu_{1-x}Ni_x)_6Sn_5$, Ni-poor variant
8	50.4 ± 1.0	3.4 ± 0.4	46.2 ± 0.9	49.3 ± 1.0	3.8 ± 0.5	46.9 ± 0.9	$(Cu_{-x}Ni_x)_6Sn_5$, Ni-poor variant
9	74.5 ± 1.5	0.2 ± 0.1	25.3 ± 0.5	74.7 ± 1.5	0.0	25.3 ± 0.5	Cu_3Sn
10	99.6 ± 2.0	0.2 ± 0.1	0.2 ± 0.1	99.5 ± 2.0	0.3 ± 0.2	0.2 ± 0.1	Cu

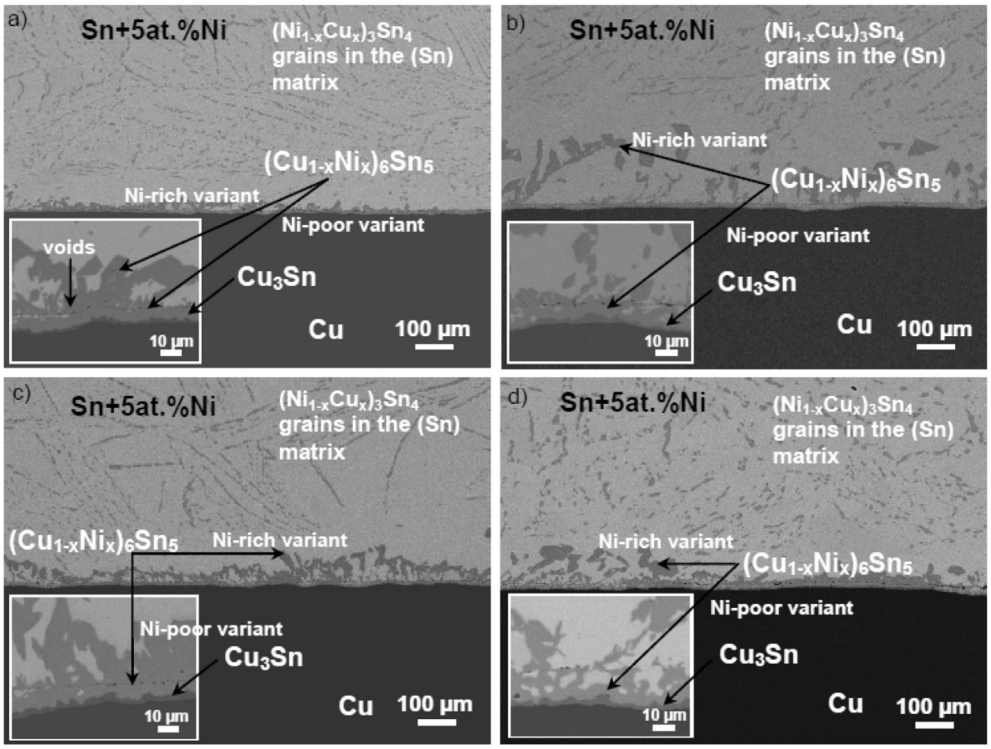

Fig. 3. SEM micrographs of the Cu/(Sn + 5 at.% Ni) diffusion couples annealed in vacuum at 215 °C for: (a) 48 h, (b) 120 h, (c) 168 h and (d) 225 h.

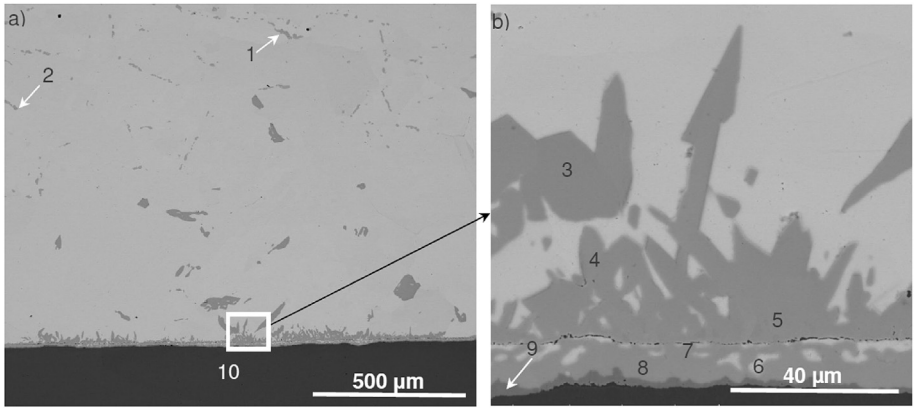

Fig. 4. SEM micrographs of the diffusion couple Cu/(Sn + 1 at.% Ni) annealed in vacuum at 215 °C for 168 h with marked points of SEM/EDS analysis, numbers 1–10: (a) overall view, (b) enlarged area marked as a white rectangle in a.

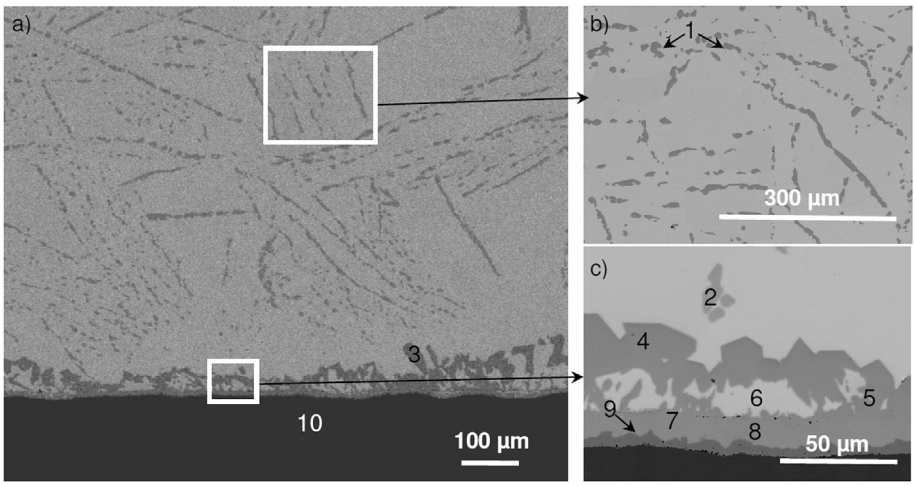

Fig. 5. SEM micrographs of the diffusion couple Cu/(Sn + 5 at.% Ni) annealed in vacuum at 215 °C for 168 h with marked points of SEM/EDS analysis, numbers 1–10: (a) overall view, (b and c) enlarged areas marked as a white rectangles in a.

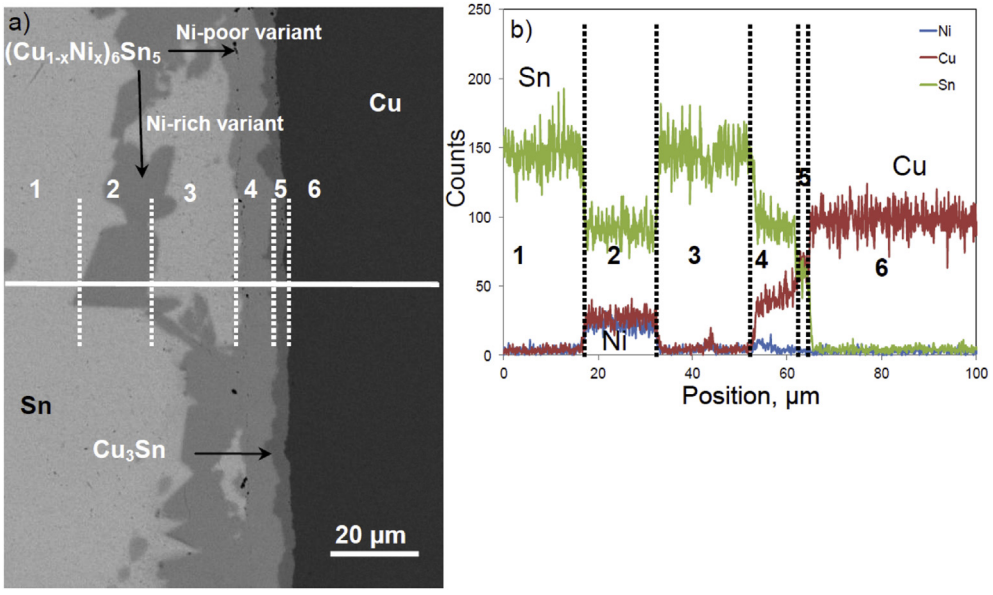

Fig. 6. SEM micrograph of the Cu/(Sn-1 at.% Ni) diffusion couple annealed in vacuum at 215 °C for 168 h (a), with corresponding EDS line scans (b). Numbers 1–6 denote particular areas of microanalysis relevant to results shown in b.

dislocations. The grains growing faster than in the classical Cu/Sn couple are exposed to stress. On the other hand, the grains of Cu_3Sn are free of the dislocations and posses round regular shapes (Fig. 8e). The selected area electron diffraction patterns unambiguously confirmed the presence of both $(Cu_{1-x}Ni_x)_5Sn_6$ and Cu_3Sn phases (Fig. 8d and e).

4. Discussion

4.1. $(Cu_{1-x}Ni_x)_6Sn_5$ phase

Independently of the nickel amount added to the (Sn,Ni) pad, in all the investigated samples $(Cu_{1-x}Ni_x)_6Sn_5$ phase growth was detected. Similar observation was made by Tsai et al. [20] concerning interaction between Cu and Sn3.5Ag solder doped with 0.1, 0.5 or 1 wt. % of Ni. In comparison to the growth of the classical Cu_6Sn_5 phase several differences were indicated in the $(Cu_{1-x}Ni_x)_6Sn_5$. First of all, the dual morphology of this phase was observed accompanied by the spalling of the rich-Ni $(Cu_{1-x}Ni_x)_6Sn_5$ phase variant. It can be only speculated in here, that the reason of the massive intermetallic spalling in the solid state can be attributed to the mechanical stresses caused by the different growth rate of IMCs.

As it was previously reported in the literature [24–26] duplex grain morphology can occur inside the intermetallic compound, where two sublayers of different shape, size or orientation of the grains can be observed. Such dual morphology is the clear evidence for Kirkendall effect within the diffusion couple [27]. It should be pointed out that in many cases, it is rather difficult to locate the position of the marker plane from the position of the voids. In such case, the grain morphology difference can provide clear indications about the marker plane.

Yoon et al. [28] observed various Cu_6Sn_5 morphologies under different experimental conditions – temperature, time and cooling; either needle-like, polyhedron-, or dodecahedron-type intermetallics were present. Although the nickel amount in the

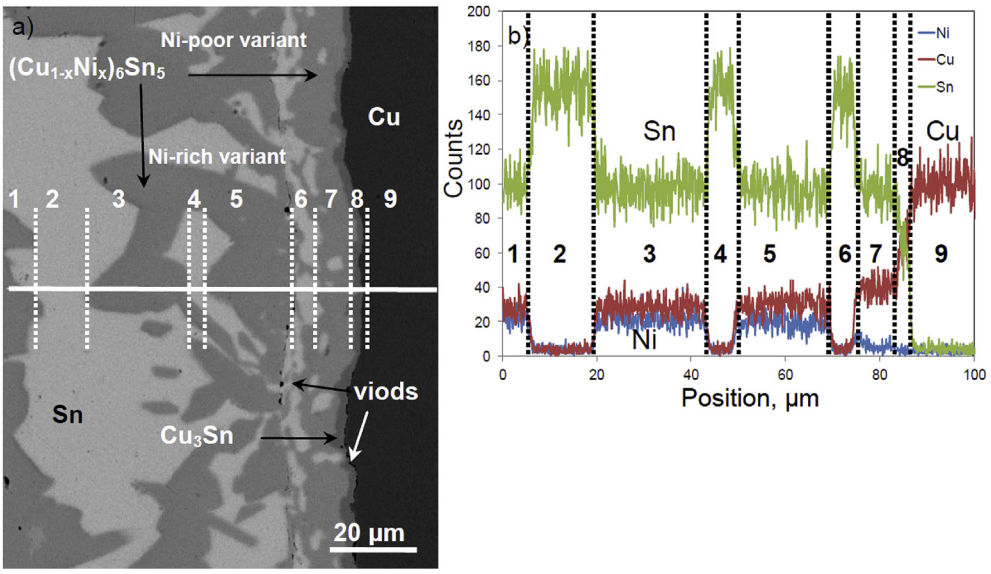

Fig. 7. Micrograph of the Cu/(Sn-5 at.% Ni) diffusion couple annealed in vacuum at 215 °C for 168 h (a), with corresponding EDS line scans (b). Numbers 1–9 denote particular areas of microanalysis relevant to results shown in b.

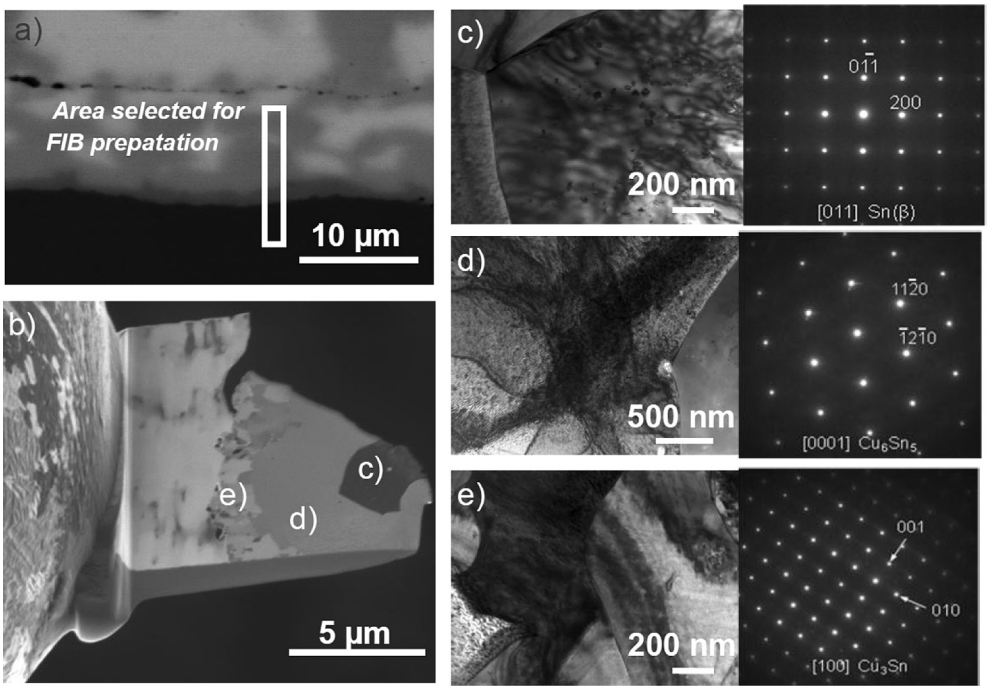

Fig. 8. SEM/FIB micrograph of the Cu/(Sn + 5 at.% Ni) diffusion couples annealed in vacuum at 215 °C for 48 h: SEM/FIB overall view of the diffusion couple (a), the final thin foil (b) where the places of further study was marked with letters c–e. TEM bright field images (c–e) together with corresponding selected area electron diffractions.

intermetallic phase changed significantly from about 12 to 20 at.%, the morphology change was not prescribed to it but to different experimental conditions (temperature, cooling speed). Two variants of the same intermetallics were observed also in Ni/Al/Ni interconnections but they did not differ morphologically between themselves [12].

Vourinen et al. [19] stated, based on the EDS measurements, that the Ni content of the $(Cu,Ni)_6Sn_5$ phase was close to that of the original Cu(Ni) alloy. For example when 1 at.% of Ni was added to Cu, the Ni content of $(Cu,Ni)_6Sn_5$ was about 1 at.%. No list of EDS data was presented in their paper, however, even this short comment points large discrepancies between our and their results. Similar results like Vourinen et al. [19] were obtained in our previous research concerning the nickel additions to copper (5 at.% of Ni) [12] where the $(Cu_{1-x}Ni_x)_6Sn_5$ phase contained 3.5–4.5 at.% Ni.

Ho et al. [29] observed dual morphology and composition of $(Cu,Ni)_6Sn_5$ in the reaction between SAC305 and Au/Pd(P)/Ni(P) surface finish on Cu. High and low nickel content phases (not specified the element amounts) possessed similar morphology as in our case. The Authors [29] also claimed that high Ni-containing $(Cu,Ni)_6Sn_5$ grew in the early stage of the soldering process and the low Ni type after longer times of interaction between solder

alloy and pads. Moreover, lower nickel $(Cu,Ni)_6Sn_5$ variant formed dense layer with some tin amount trapped within it, which was also observed in particular places in our study (compare Figs. 4b, 6a and 7a). Ho et al. [29] prescribed the dual morphology of $(Cu,Ni)_6Sn_5$ phase to different reaction systems claiming that the higher Ni containing variant resulted from the solder/Ni(P) reaction, while the lower one from the solder/Cu reaction. However, in the present study similar morphology is created although the (Sn,Ni) pad with only 1–5 at.% of Ni served as the nickel source. Liu et al. [22] showed such dual morphology as well, providing also the composition data being relevant to our experimental data. Tsai et al. [20] reported similar microstructure as previous cited researchers commenting that the low Ni variant was formed in the liquid state, while the higher containing nickel variant was formed during the solidification of the molten solder. Nevertheless, it should be stressed that in all above mentioned papers [20,22,29] liquid–solid interaction took place in comparison to this work.

In the present study at the interface of two sublayers the voids were clearly distinguished across the line within $(Cu_{1-x},Ni)_6Sn_5$ phase (Figs. 2 and 3), being the manifestation of the Kirkendall effect (Kirkendall plane). These voids are formed in the case of the large difference in mobility of the species, because not enough sites are available to consume the vacancies that go in the opposite direction to the faster diffusing species. For example, in the classical Cu/Sn diffusion couple experiment it was estimated that copper is 32 times faster than Sn through the Cu_3Sn phase [30].

Tsai reported that the voids within the $(Cu_{1-x},Ni)_6Sn_5$ phase were formed during the reflow in the liquid state, while the part of the phase formed during solid state aging was free of voids [20]. However, these voids were of different nature as they are the areas where the liquid solder was trapped. Nevertheless, Ho et al. [29] evidenced the nanovoids between $(Cu,Ni)_6Sn_5$ (high Ni) and $(Cu,Ni)_6Sn_5$ (low Ni), demonstrating their contribution to the reduction in the joint.

The present study also allows to compare the Cu/(Sn,Ni) (1 and 5 at.% Ni) microstructure with classical Cu/Sn diffusion couple one revealing that the increase of the Ni content in the Sn caused that much more rapid growth of $(Cu_{1-x}Ni_x)_6Sn_5$ phase within the reaction zone (Figs. 2 and 3). As it was presented previously in Ref. [11] the nickel addition to the copper resulted in much faster growth of the $(Cu_{1-x}Ni_x)_6Sn_5$ phase and was attributed to the substantial contribution of grain boundary diffusion during the joining process. Moreover, Tsai et al. also reported that during the interaction between Cu and Sn3.5Ag solder doped with Ni, the kinetics of the $(Cu_{1-x}Ni_x)_6Sn_5$ phase formation became much faster with increasing the Ni addition [20].

The selected area electron diffraction patterns in TEM confirmed the presence of the $(Cu_{1-x}Ni_x)_6Sn_5$ phase (Fig. 8d). What is more, the measured distances gave a good agreement with the lattice parameters of the Cu_6Sn_5 phase. Therefore, it can be concluded that the nickel atoms substitution to the copper ones does not change the crystallographic structure of this phase. The similar observation was presented by Tsai et al. [20], who noted that Ni addition to the Sn–Ag solder caused only the changes in the chemical composition of the Cu_6Sn_5 phase and not in its crystal structure.

4.2. Cu_3Sn phase

From the SEM and TEM microstructure and chemical composition characterization results presented in this study, it was found that the Cu_3Sn phase was also formed in all examined samples.

The Cu_3Sn intermetallic phase was formed as the wavy continuous layer near to the Cu pad (Figs. 2 and 3). The shape of this intermetallic compound was close to that observed in the classical Cu/Sn system as well as in the (Cu + 1 at.%Ni)/Sn [18,19].

Moreover, the EDS/SEM quantitative analysis (Table 1) revealed that no Ni was present in the Cu_3Sn even for the higher content of the nickel in the Sn pad (5 at.%) and long time of annealing (168 h). The same situation was discussed by Tsai et al. [20], who observed the Cu_3Sn phase formation between Cu and Cu_6Sn_5 phase after solid-state aging of the Cu and Sn3.5Ag solder with Ni addition at 150 °C for 1000 h.

Furthermore, many voids, along this phase appeared after long time of annealing (168 h and longer) – see magnified box in Fig. 2d. The Cu_3Sn phase porosity was previously reported by Paul et al. [18], in Cu-1 at.% Ni/Sn couples. According to their calculations in Cu/Sn couple no stable Kirkendall plane formed inside the Cu_3Sn phase. It was explained by the fact that the purity of the diffusion couple end members is the factor that may influence the diffusion fluxes and therefore to initiate the creation of Kirkendall plane inside Cu_3Sn. As this is not a case here (high purity of the end members) the voids in both $(Cu,Ni)_6Sn_5$ and Cu_3Sn were placed along the line (Kirkendall plane).

Contrary to $(Cu_{1-x}Ni_x)_6Sn_5$ phase growth, the observed changes in amount of the Cu_3Sn were not so significant with increasing nickel concentration in tin (Figs. 2 and 3). It is worth noting that the largest difference in the thickness of the Cu_3Sn phase from about 2 μm to 10 μm was observed between the couples annealed for 48 and 120 h. Further prolongation of the experiment did not result in so significant changes.

Studies on Cu/Sn diffusion couples performed by Tu and Thompson [31–33] demonstrated that below 50 °C only the stable Cu_6Sn_5 phase nucleated and no Cu_3Sn phase was evidenced. Above this temperature formation of both phases was observed. Furthermore, it was showed that the formation of Cu_3Sn [30] in Cu/Cu_6Sn_5 diffusion couples in the temperature range from 115 to 150 °C takes place at least partly at the expense of Cu_6Sn_5 and its absence in the samples is correlated with the nucleation problems. It was stated that the phases with high fluxes of diffusing species are favored and can suppress the growth of other phases.

At low temperatures noble and near-noble metals (Cu) can diffuse interstitially in-group IV elements, such as Sn, and also the grain boundary diffusion takes place [34]. Contrary to this the vacancy-mediated volume diffusion predominates at higher temperatures. At temperatures above 100 °C tin is the fastest diffusing element in Cu_6Sn_5 while the copper in Cu_3Sn [19]. Yu et al. [35] suggested the increase of the driving force for the diffusion of Sn through Cu_6Sn_5 with increasing nickel content in the phase.

4.3. Diffusion path

The chemical composition changes collected in Table 1 across the diffusion couple allowed to draw the diffusion path on the isothermal section of the equilibrium phase diagram calculated in Ref. [36] for 220 °C (dotted line in Fig. 9a). Fig. 9b shows the schematic representation of the microstructure drawn based on its course and the rules given by Clark [37]. As the chemical composition of phases formed in the both investigated diffusion couples differed slightly, only the diffusion path for the Cu/(Sn + 5 at.% Ni) couple was presented.

The diffusion path starts in the (Sn) + Ni_3Sn_4 two phase field (one of the end members used in the diffusion couple), then crosses the Ni_3Sn_4 phase field and again goes back through the two-phase field (Sn) + Ni_3Sn_4. The representation of such course are the $(Ni_{1-x}Cu_x)_3Sn_4$ phase precipitates within the (Sn) matrix. Next the path runs through the three phase field (Sn) + Ni_3Sn_4 + Cu_6Sn_5 – in the tin matrix the $(Ni_{1-x}Cu_x)_3Sn_4$ $(Cu_{1-x}Ni_x)_6Sn_5$ precipitates are present. Then it enters to the two-phase field (Sn) + Cu_6Sn_5 (in the tin matrix the $(Cu_{1-x}Ni_x)_6Sn_5$ phase precipitates) and afterward to the Ni-rich $(Cu,Ni)_6Sn_5$ phase field. After that the path goes back to

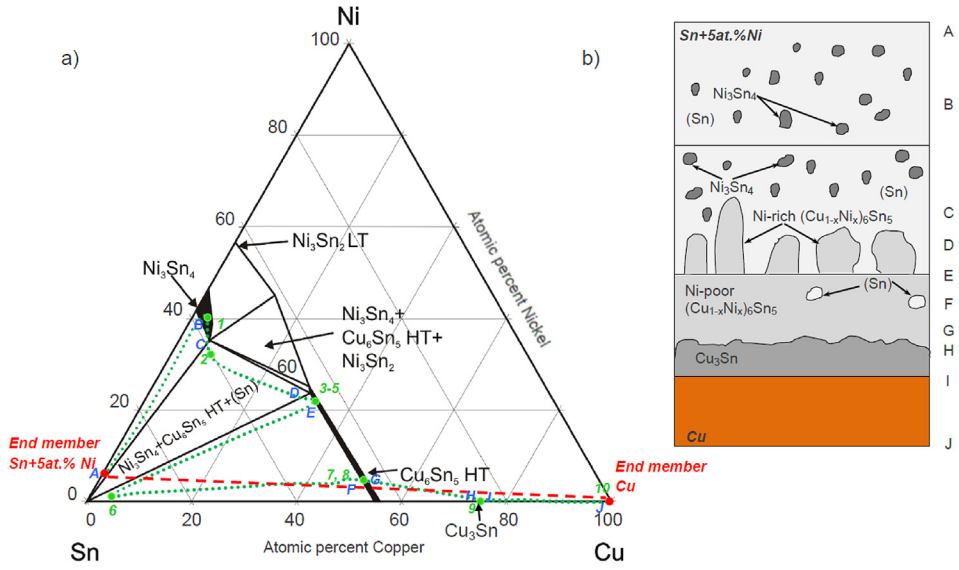

Fig. 9. Isothermal section of Cu–Ni–Sn phase equilibrium diagram at 220 °C [36], axes in at.%. The green points no. 1–10 correspond to the SEM/EDS analysis listed in Table 1. The diffusion path for Cu/(Sn + 5 at.% Ni) was marked with dotted line, while the dashed line represents the tie-line between applied end-members (a). Schematic diagram of the microstructure drawn based on the rules given by Clark [37]. (For interpretation of the references to colour in this figure legend, the reader is referred to the web version of this article.)

the two-phase field (Sn) + Cu_6Sn_5 – in the microstructure the tin is trapped within the $(Cu_{1-x}Ni_x)_6Sn_5$ phase. Subsequently the path crosses the Ni-poor $(Cu,Ni)_6Sn_5$ phase field, which appears as a continuous layer. At the end Cu_3Sn phase field is crossed by the diffusion path, finishing in Cu end member, which can be seen as layer of Cu_3Sn between the $(Cu_{1-x}Ni_x)_6Sn_5$ and Cu. Schematic diagram of microstructure (Fig. 9b) gives a good agreement with SEM observations (Figs. 2–7).

The contradictory results were obtained by Vourinen [19], where the diffusion path did not passed across the stability region of Cu_3Sn phase and so it was not observed in their samples.

The lack of Cu_3Sn phase was also observed by Tu et al. [31] in their experiment and it was ascribed to the problems with nucleation. In the light of our previous study [10] concerning diffusion soldered interconnections ((Cu-5 at.%Ni)/Sn/(Cu-5 at.%Ni)) this statement holds, as the barrier of nickel concentrated at the Cu(Ni)/$(Cu_{1-x}Ni_x)_6Sn_5$ was detected, and no Cu_3Sn phase was present. On the other hand, presented here TEM studies of the Cu/(Sn + 5 at.% Ni) diffusion couples did not reveal the presence of nickel barrier, and so the Cu_3Sn was created.

5. Conclusions

The presented diffusion couple experiment together with the microstructure and phase composition data contribute to the knowledge in the field of phase transformations in ternary Cu–Ni–Sn system [38–42], considered as one of the most important in the soldering.

The scanning and transmission electron microscopy examination on Cu/(Sn,Ni) diffusion couples with the 1 and 5 at.% of Ni addition prepared at 215 °C in vacuum for various time (48, 120, 168 and 225 h) allowed to detect three intermetallic compounds: $(Cu_{1-x}Ni_x)_6Sn_5$ and Cu_3Sn and $(Ni_{1-x}Cu_x)_3Sn_4$. The $(Cu_{1-x}Ni_x)_6Sn_5$ evidenced strong manifestation of Kirkendall effect by its dual morphology. This phase took the form of either the discontinuous layer closer to the copper side or various shaped precipitates (needles or faced) from the tin–nickel side. These precipitates detached from the interface and were localized even up to 100 μm from it. Such differences in microstructure were accompanied by the chemical composition fluctuations, which varied from 3.4 to 7.2 at.% of Ni in the layer and from 17.5 to 22.3 at.% of Ni in precipitates. The growth of the $(Cu_{1-x}Ni_x)_6Sn_5$ phase in Cu/(Sn,Ni) couple was faster than Cu_6Sn_5 in Cu/Sn. However, its growth was slower than in the case of (Cu,Ni)/Sn couple. On the other hand, the Cu_3Sn phase forming wavy layer at the Cu/$(Cu_{1-x}Ni_x)_6Sn_5$ appeared in the diffusion couples even for larger amounts (5 at.%) of nickel added into tin before the experiment which was not previously reported.

Acknowledgments

The research was financially supported by the National Science Centre under the grant no. 2011/03/B/ST8/06158. The TEM and EDS/SEM studies were performed in the Accredited Testing Laboratories at the Institute of Metallurgy and Materials Science of the Polish Academy of Sciences. The SEM research was carried out at the Institute of Materials Engineering, Cracow University of Technology.

References

[1] Directive on the restriction of the use of certain hazardous substances in electrical and electronic equipment. Directive 2002/95/EC Off J Eur Union 13 February 2003.
[2] Advanced solder materials for high-temperature application – their nature, design, process and control in a multiscale domain. Memorand Understand 2006:1–15. COST Action MP0602.
[3] Yoon JW, Noh BI, Yoon JH, Kang HB, Jung SB. Sequential interfacial intermetallic compound formation of Cu_6Sn_5 and Ni_3Sn_4 between Sn–Ag–Cu solder and ENEPIG substrate during a reflow process. J Alloys Compd 2011;509:L153–6.
[4] Wang YW, Chang CC, Kao CR. Minimum effective Ni addition to SnAgCu solders for retarding Cu_3Sn growth. J Alloys Compd 2009;478:L1–4.
[5] Nishikawa N, Piao JY, Takemoto T. Interfacial reaction between Sn–0.7Cu (–Ni) solder and Cu substrate. J Electron Mater 2006;35:1127–32.
[6] Wang CH, Shen HT. Effects of Ni addition on the interfacial reactions between Sn–Cu solders and Ni substrate. Intermetallics 2010;18:616–22.
[7] Zieba P, Wojewoda J. Application of diffusion soldering in lead-free interconnection technology. Recent Res Dev Mater Sci Res Signpost, Kerala 2003;4:261–82.

[8] Wojewoda J. Solid state transformations in Cu/In–48Sn/Cu diffusion soldered interconnections. Solid State Phenom 2008;138:165–74.
[9] Skrzyniarz P, Sypien A, Wojewoda-Budka J, Filipek R, Zieba P. Microstructure and kinetics of intermetallic phases growth in Ag/Sn/Ag joint obtained as the results of diffusion soldering. Arch Metall Mater 2010;55:123–30.
[10] Wierzbicka-Miernik A, Wojewoda-Budka J, Litynska-Dobrzynska L, Kodentsov A, Zieba P. Morphology and chemical composition of Cu/Sn/Cu and Cu(5at% Ni)/Sn/Cu(5at% Ni) interconnections. Sci Technol Weld Join 2012;17(1):32–5.
[11] Wierzbicka-Miernik A, Miernik K, Wojewoda-Budka J, Szyszkiewicz K, Filipek R, Litynska-Dobrzynska L, et al. Growth kinetics of the intermetallic phase in diffusion-soldered (Cu-5 at.%Ni)/Sn/(Cu-5 at.%Ni) interconnections. Mater Chem Phys 2013;142:682–5.
[12] Lopez GA, Sommadossi S, Gust W, Mittemeijer EJ, Zieba P. Phase characterization of diffusion soldered Ni/Al/Ni interconnections. Interface Sci 2002;10:13–9.
[13] Sommadossi S, Fernández Guillermet A. Interface reaction systematics in the Cu/Ine48Sn/Cu system bonded by diffusion soldering. Intermetallics 2007;15:912–7.
[14] López GA, Sommadossi S, Zieba P, Gust W, Mittemeijer EJ. Kinetic behaviour of diffusion-soldered Ni/Al/Ni interconnections. Mater Chem Phys 2002;78:459–63.
[15] Sommadossi S, Gust W, Mittemeijer EJ. Characterization of the reaction process in diffusion-soldered Cu/In–48 at.% Sn/Cu joints. Mater Chem Phys 2003;77:924–9.
[16] Litynska L, Wojewoda J, Zieba P, Faryna M, Gust W, Mittemeijer EJ. Characterization of interfacial reactions in Cu/In/Cu joints. Microchim Acta 2004;145:107–10.
[17] Bader S, Gust W, Hieber H. Rapid formation of intermetallic compounds by interdiffusion in the Cu–Sn and Ni–Sn systems. Acta Metall Mater 1995;43(1):329–37.
[18] Paul A. Doctoral dissertation. Technical University of Eindhoven; 2004.
[19] Vuorinen V, Laurila T, Mattila T, Heikinheimo E, Kivilahti J. Solid-state reactions between Cu(Ni) alloys and Sn. J Electron Mater 2007;36(10):1355–62.
[20] Tsai JY, Hu YC, Tsai CM, Kao CR. A study on the reaction between Cu and Sn3.5Ag solder doped with small amounts of Ni. J Electron Mater 2003;32:1203–8.
[21] Gao F, Takemoto T, Nishikawa H. Effects of Co and Ni addition on reactive diffusion between Sn–3.5Ag solder and Cu during soldering and annealing. Mat Sci Eng A 2006;420:39–46.
[22] Liu CS, Ho CE, Peng CS, Kao CR. Effects of joining sequence on the interfacial reactions and substrate dissolution behaviors in Ni/Solder/Cu joints. J Electron Mater 2011;40:1912–20.
[23] Dinsdale AT, Watson A, Kroupa A, Vrestal J, Zemanova A, Vizdal J. Version 3.1 of the "COST531" database for the lead-free solders.
[24] Gulpen JH, Kodentsov AA, Van Loo FJJ. Growth of silicides on Ni–Si and Ni–SiC bulk diffusion couples. Z Met 1995;86:530–9.
[25] Van Beek JA, Stolk SA, Van Loo FJJ. Multiphase diffusion in the system Fe–Sn and Ni–Sn. Z Met 1982;73:439–44.
[26] Przybylski K, Smeltzer WW. High temperature oxidation mechanism of CoO to Co_3O_4. J Electrochem Soc 1981;128:897–902.
[27] Paul A. Growth mechanism of phases, Kirkendall voids, marker plane position, and indication of the relative mobilities of the species in the interdiffusion zone. J Mater Sci Mater Electron 2011;22:833–7.
[28] Yoon JW, Kim SW, Jung SB. Effects of reflow and cooling conditions on interfacial reaction and IMC morphology of Sn–Cu/Ni solder joint. J Alloy Compd 2006;415:56–61.
[29] Ho CE, Wang SJ, Fan CW, Wu WH. Optimization of the Ni(P) thickness for an ultrathin Ni(P)-based surface finish in soldering applications. J Electron Mater 2014;43:16–25.
[30] Paul A, Ghosh C, Boettinger WJ. Diffusion parameters and growth mechanism of phases in the Cu–Sn system. Metall Mater Trans A 2011;42:952–63.
[31] Tu KN. Interdiffusion and reaction in bimetallic Cu–Sn thin films. Acta Metall 1973;21:347–54.
[32] Tu KN, Thompson RD. Kinetics of interfacial reaction in bimetallic Cu–Sn thin films. Acta Metall 1982;30:947–52.
[33] Tu KN. Cu/Sn interdiffusion reactions: thin film case vs bulk case. Mater Chem Phys 1996;46:217–23.
[34] Oh M. Doctoral dissertation. Lehigh University; 1994.
[35] Yu H, Vuorinen V, Kivilahti JK. In: The proceedings of the 2006 IEEE/EIA CPMT electronic component and technology conference (ECTC06), San Diego, California, USA; May 29–June 1, 2006.
[36] Schmetterer C, Flandorfer H, Luef CH, Kodentsov A, Ipser H. Cu–Ni–Sn: a key system for lead-free soldering. J Electron Mater 2009;38(1):10–24.
[37] Clark JB. Conventions for plotting the diffusion paths in multiphase ternary diffusion couples on the isothermal section of a ternary phase diagram. Trans Metall Soc AIME 1963;227:1250–1.
[38] Chakrabarti DJ, Laughlin DE, Chen SW, Chang YA. In: Nash P, editor. Phase diagrams of binary nickel alloys. Materials Park, OH: ASM International; 1991.
[39] Massalski TB, Okamoto H, Subramanian PR, Kacprzak L. Binary alloy phase diagrams. Materials Park, OH: ASM International; 1991.
[40] Saunders N, Miodownik AP. Bull Alloy Phase Diagr 1990;11:278.
[41] Nash A, Nash P. Bull Alloy Phase Diagr 1985;6:350.
[42] Ghosh G. Thermodynamic modeling of the nickel–lead–tin system. Metall Mater Trans 1999;30A:1481–94.